Dynamic Control Set-Model Predictive Control for Field-Oriented Control of VSI-PMSM

Shuai Wang and Dewei(David) Xu
Department of Electrical and Computer Engineer
Ryerson University, Toronto, ON, Canada
Email: wangshuai@ryerson.ca, dxu@ryerson.ca

Chushan Li
ZJU-UIUC Institute
Haining, 314400, Zhejiang Province, China
Email: chushan@intl.zju.edu.cn

***Abstract*—In this digest, a novel Model Predictive Control scheme is proposed for 2L-VSI PMSM drive system. Even though standard FCS-MPC can lead to low switching frequency, but it degrades the steady state performance, while MPC with duty cycle reduces the current and torque ripples at expense of high switching frequency. To mollify the contradiction between the steady-state performance and the switching frequency, the proposed approach can move the switching instant from sampling instant to any instant within a sampling interval. But variable switching instant also introduces infinite candidate control actions, which can compose a dynamic control set. To capture the optimal control action, variable switching instant is transformed as vectoral form, and the convey quadratic relationship between objective function and variable switching instant is derived. Based on it, an online optimization procedure is established. Finally, the test results show that the proposed approach can reach a balance between steady-state performance and switching frequency.**

Keywords— permanent magnet synchronous motor(PMSM), Model Predictive Control(MPC), variable switching instant, online optimization

I. INTRODUCTION

Field-oriented Control(FOC) and Direct Torque Control (DTC) can be considered as two most well-established control methods for permanent magnet synchronous motor(PMSM) fed by voltage source inverter (VSI)[1]. Different from DTC, the classic FOC schemes is a cascaded scheme based on proportional-integral plus pulse width modulator (PI-PWM), such Space vector PWM(SVM) or Sine PWM(SPWM)[]. Under this scheme, the delay of PI controller and modulator will degrade dynamic response. Fortunately, thanks to the advent of fast and powerful micro-processors, Finite Control Set Model Predictive Control(FCS-MPC) has been adopted to the FOC scheme to replace PI-PWM, because that MPC can integrate the current regulation as well as PWM output. Moreover, without any modulator, MPC can directly manipulating the switching state according to the solution of MPC optimization problem, which leads to a high dynamic response. Besides that, at high sampling rate, the output switching state can keep consistent during several sampling intervals, which can cause less switching frequency. Thus, FCS-MPC can be featured as low switching frequency under high sampling rate, that is the reason why MPC become more promising in the medium- and high-voltage drives field[2].

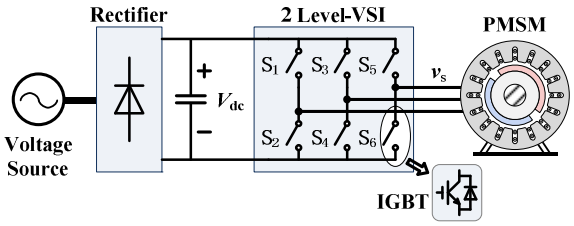

Fig. 1. Simplified schematic of VSI-PMSM.

But, for FCS-MPC, as the switching instant is always fixed at the sampling instant. Only one switching state employed within a sampling interval and fixed switching instant will result in uncontrollable peak-peak values of d- and q-axis current within a sampling interval, which will deliver more serious torque ripple and higher current distortion. To improve the steady-state performance, duty cycle modulation was introduced into FCS-MPC in [3]-[8]. By inserting a null switching state and adjusting the duration of active switching state, the peak-peak values of d- and q-axis current can be reduced significantly. Moreover, many modified FCS-MPCs adopt more switching states modulation in [9][10], in which the switching pattern within one sampling interval includes two arbitrary switching states, rather than restricts to active- plus null-switching state. The flexibility of combination of switching states can deliver better steady-state performance than MPCs with duty cycle. Consequently, above works have proved the effectiveness of employing more switching states. Now there is a tradeoff. For duty cycle-based and more switching states-based MPC, as multiple switching states are inserted into one sampling interval, and at least two switching behaviors will occur at every sampling instant as well as the interior of every sampling interval. Therefore, MPCs with modulator will cause higher switching frequency than the traditional one. Apparently, high steady-state performance and low switching frequency is a pair of contradiction.

This paper aim to propose a novel Dynamic Control Set-MPC to reach a balance between the steady-state performance and switching frequency. Firstly, variable switching instant will be adopted into the MPC scheme, and the relationship between variable switching instant and the future behavior of PMSM will be established, which will facilitate to formulate the MPC optimization problem. To capture the optimal switching pattern, a solving procedure via finite enumerate and evaluation will be derived. Finally, the experiments are carried out and some conclusions are summarized.

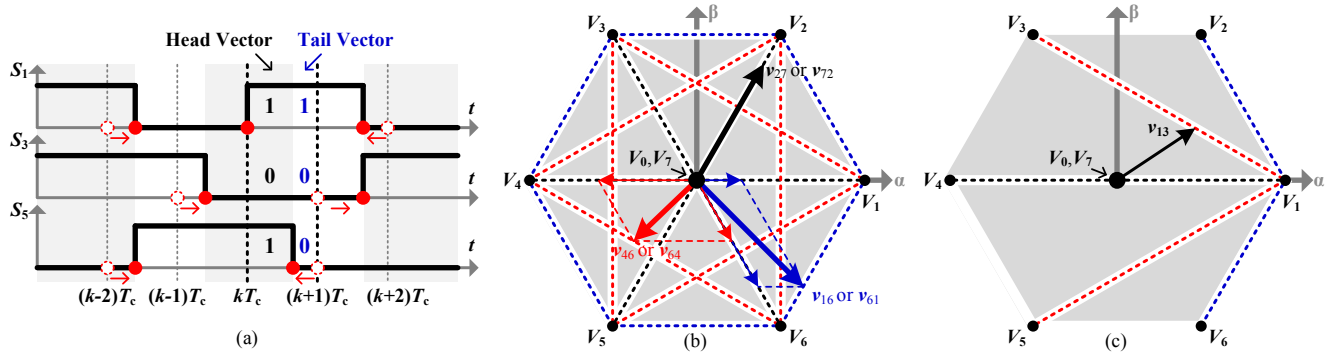

Fig. 2. Switching signal and vector diagram for variable switching instant.

II. Physical Model

In this section, the variable switching instant will be illustrated from the view of space vector, which can help revealing the relationship between variable switching instant and PMSM's future behaviors. Based on it, the predictive model of the proposed approach will be established which will facilitate to formula the MPC optimization problem.

A. Variable Switching Point

Schematic diagram of VSI-PMSM can be found in Fig.1, where 2-Level VSI has eight switching states $\{S_1, S_3, S_5\}$, S_1, S_3, $S_5 \in \{0,1\}$, which can be expressed in vectorial form by

$$\boldsymbol{V}_n = \frac{2}{3}V_{\mathrm{dc}}\left(S_1 + S_3 e^{\mathrm{j}\frac{2}{3}\pi} + S_5 e^{-\mathrm{j}\frac{2}{3}\pi}\right) = \begin{cases} \frac{2}{3}V_{\mathrm{dc}} e^{\mathrm{j}\frac{n-1}{3}\pi} & n = 1,\ldots 6 \\ 0 & n = 0,7 \end{cases} \quad (1)$$

where V_{dc} is the DC link voltage; n=0,1,…,7. $\boldsymbol{V}_1$~$\boldsymbol{V}_6$ and $\boldsymbol{V}_0$, $\boldsymbol{V}_7$ can be referred to as active vector and null vector respectively.

For variable switching point, by moving the switching instant to the middle of the control interval as shown in Fig.2(a), two different switching states will appear in one control interval, which leads to more active vectors or null vectors employed within one control interval. But, in order to keep low switching frequency, two restricting condition should be set in following: ***a)*** Only one switching instant takes place within an arbitrary control interval $[kT_c, (k+1)T_c)$ at the most, which leads to two vectors employed within one control interval at the most, where the vector employed before switching instant is referred to as head vector, and the other is referred to as tail vector. ***b)*** The head vector in the current control period must be identical to the tail vector in the last control period, as shown in Fig.2(a).

From the view of vector, the voltage vector with respect to variable switching instant is regarded as the synthesis of head vector and tail vector, while the synthesizing vector trajectory is determined by the combination of head vector and tail vector. Specifically, if head vector or tail vector is a null vector either, the synthesizing vector trajectory is the **Snow-shape** as $\boldsymbol{v}_{72}$ in Fig.2(b), and the lengths of them are controllable, but the angles of them just locate in six fixed directions associate with 6 active vectors. If the head active vector and the tail active vector are adjacent, then the synthesizing vector trajectory are the **Hexagon**, as $\boldsymbol{v}_{16}$ in Fig.2(b). On the other hand, if the head active vector and the tail active vector are neither adjacent nor align, then the synthesizing vector's terminal will locate on the **Star of David**, as $\boldsymbol{v}_{46}$ in Fig.2(b). From Eq.(1), the expressions of them in vectorial form can be expressed as follows

$$\boldsymbol{v}_{mn}(t_{\mathrm{h}}) = \frac{t_{\mathrm{h}}}{T_{\mathrm{c}}}\boldsymbol{V}_m + \frac{T_{\mathrm{c}} - t_{\mathrm{h}}}{T_{\mathrm{c}}}\boldsymbol{V}_n \quad (2a)$$

$$\boldsymbol{V}_i = \begin{cases} \frac{2}{3}V_{\mathrm{dc}} e^{\mathrm{j}\frac{i-1}{3}\pi} & i = 1,\ldots 6 \\ 0 & i = 0,7 \end{cases} \quad (2b)$$

where $t_{\mathrm{h}} \in [0,\ T_{\mathrm{c}}]$ is the time duration of the head vector, which can be regarded as the switching instant in a control interval.

Consequently, for these kinds of vectors, both length and angle can be adjusted by the time duration t_{h} finely.

B. Predictive Model of PMSM

Establish the rotating d-q coordinates and align the rotor flux $\boldsymbol{\Psi}_{\mathrm{r}}$ on the d-axis. The stator voltage equation of PMSM in the rotating d-q coordinates can be expressed as follows

$$\begin{cases} {v_{mn}}^{\mathrm{d}} = R_{\mathrm{s}} i_{\mathrm{sd}} + L_{\mathrm{d}} \dfrac{\mathrm{d}}{\mathrm{d}t} i_{\mathrm{sd}} - \omega_{\mathrm{r}} L_{\mathrm{q}} i_{\mathrm{sq}} \\ {v_{mn}}^{\mathrm{q}} = R_{\mathrm{s}} i_{\mathrm{sq}} + L_{\mathrm{q}} \dfrac{\mathrm{d}}{\mathrm{d}t} i_{\mathrm{sq}} + \omega_{\mathrm{r}} L_{\mathrm{d}} i_{\mathrm{sd}} + \omega_{\mathrm{r}} \psi_{\mathrm{f}} \end{cases} \quad (3)$$

where R_{s} is the stator resistance; ψ_{f} is the permanent magnet flux modulus; L_{d} and L_{q} are the direct and quadrature stator inductance respectively, $L_{\mathrm{d}} \leq L_{\mathrm{q}}$; ω_{r} is the rotor flux angular velocity; i_{sd} and i_{sq} are the d-axis and q-axis projections of stator current $\boldsymbol{i}_{\mathrm{s}}$; ${v_{mn}}^{\mathrm{d}}$ and ${v_{mn}}^{\mathrm{q}}$ are the d-axis and q-axis projections of vector $\boldsymbol{v}_{mn}$.

In a subsequent step, Eq.(3) can be discretized via Euler approximation, and then the predictive model of PMSM can be expressed as follows

$$\begin{cases} i_{\mathrm{sd}}{}^{mn}(k+1)=(1-\dfrac{T_{\mathrm{c}}R_{\mathrm{s}}}{L_{\mathrm{d}}})i_{\mathrm{sd}}(k)+\dfrac{T_{\mathrm{c}}}{L_{\mathrm{d}}}\left[v_{mn}{}^{\mathrm{d}}-e_{\mathrm{sd}}(k)\right] \\ i_{\mathrm{sq}}{}^{mn}(k+1)=(1-\dfrac{T_{\mathrm{c}}R_{\mathrm{s}}}{L_{\mathrm{q}}})i_{\mathrm{sq}}(k)+\dfrac{T_{\mathrm{c}}}{L_{\mathrm{q}}}\left[v_{mn}{}^{\mathrm{q}}-e_{\mathrm{sq}}(k)\right] \end{cases} \tag{4a}$$

$$\begin{cases} e_{\mathrm{sd}}(k)=-\omega_{\mathrm{r}}(k)L_{\mathrm{q}}i_{\mathrm{sq}}(k) \\ e_{\mathrm{sq}}(k)=\omega_{\mathrm{r}}(k)\left[L_{\mathrm{d}}i_{\mathrm{sd}}(k)+\psi_{\mathrm{f}}\right] \end{cases} \tag{4b}$$

where T_{c} is the control period; $i_{\mathrm{sd}}{}^{mn}(k+1)$ and $i_{\mathrm{sq}}{}^{mn}(k+1)$ are the predictions of i_{sd} and i_{sq} with respect to $\boldsymbol{v}_{\mathrm{s}}=\boldsymbol{v}_{mn}$ at instant $(k+1)T_{\mathrm{c}}$; $i_{\mathrm{sd}}(k)$ and $i_{\mathrm{sq}}(k)$ are the sampling quantities of i_{sd} and i_{sq} at instant kT_{c}.

III. Proposed Approach

A. MPC Optimization Problem

From restricting condition ***b***, the head vector $\boldsymbol{V}_{m'}$ is given at any sampling period. Geometrically, the of all available vector's terminals are located at five radial lines available voltage vectors, and the start points concentrate at the terminal of $\boldsymbol{V}_{m'}$, as shown in Fig.1(c). Collect all available vectors, and establish the control-set as follows

$$DSC=\left\{[n,t_{\mathrm{h}}]\left|\begin{array}{l}\boldsymbol{v}_{m'n}=\dfrac{t_{\mathrm{h}}}{T_{\mathrm{c}}}\boldsymbol{V}_{m'}+\dfrac{T_{\mathrm{c}}-t_{\mathrm{h}}}{T_{\mathrm{c}}}\boldsymbol{V}_{n}; \\ m'=n_{\mathrm{p}}\ \ n=0,...,7;\ n\neq m';t_{\mathrm{h}}\in[0,T_{\mathrm{c}}]\end{array}\right.\right\} \tag{5}$$

where n_{p} is tail vector's index at the last sampling interval. Since $\boldsymbol{V}_{m'}$ is variable at different sampling period, the control-set Eq.(5) is dynamic.

In order to realize the stator current tracking control, define the objective function as follows

$$g_{mn}=\left|\boldsymbol{i}_{\mathrm{s}}^{\mathrm{ref}}-\boldsymbol{i}_{\mathrm{s}}{}^{m'n}(k+1)\right|^2 \tag{6}$$

where $\boldsymbol{i}_{\mathrm{s}}^{\mathrm{ref}}$ is the reference of stator current $\boldsymbol{i}_{\mathrm{s}}$, $\boldsymbol{i}_{\mathrm{s}}^{\mathrm{ref}}=i_{\mathrm{sd}}{}^{\mathrm{ref}}+\mathrm{j}i_{\mathrm{sq}}{}^{\mathrm{ref}}$; $\boldsymbol{i}_{\mathrm{s}}{}^{mn}(k+1)=i_{\mathrm{sd}}{}^{mn}(k+1)+\mathrm{j}i_{\mathrm{sq}}{}^{mn}(k+1)$.

By taking into account the predictive model Eq.(4), the dynamic control-set Eq.(5) and the objective function Eq.(6), the MPC optimization problem can be formulated as follows

$$\begin{aligned}&\underset{[n,t_{\mathrm{h}}]}{\text{minimize}}\ \ g=\left|\boldsymbol{i}_{\mathrm{s}}^{\mathrm{ref}}-\boldsymbol{i}_{\mathrm{s}}{}^{m'n}(k+1)\right|^2 \\ &\text{subject to}\ \ \text{Eq.}(4); \\ &\qquad n=0,1,\ ...,\ 7;\ t_{\mathrm{h}}\in[0,\ T_{\mathrm{c}}]\end{aligned} \tag{7}$$

The solution of Eq.(7) can be denoted as $[n', t_{\mathrm{h}}']$. Since the number of elements in DCS is countless, it is difficult for the digital controller to enumerate and evaluate infinite objective functions for all elements in DCS. In the following, the MPC optimization problem Eq.(7) will be transformed, in order to find the solution of Eq.(7) via finite enumerations and evaluations online.

B. Solving Algorithm for the Optimization Problem

From Eq.(5), the expression of $\boldsymbol{i}_{\mathrm{s}}^{\mathrm{ref}}-\boldsymbol{i}_{\mathrm{s}}{}^{mn}(k+1)$ can be derived as follows

$$\boldsymbol{i}_{\mathrm{s}}^{\mathrm{ref}}-\boldsymbol{i}_{\mathrm{s}}{}^{m'n}(k+1)=\boldsymbol{I}-t_{\mathrm{h}}\boldsymbol{W}_{m'n} \tag{8a}$$

where

$$\begin{aligned}\boldsymbol{I}=&[i_{\mathrm{sd}}^{\mathrm{ref}}-(1-\frac{T_{\mathrm{c}}R_{\mathrm{s}}}{L_{\mathrm{d}}})i_{\mathrm{sd}}(k)+\frac{T_{\mathrm{c}}}{L_{\mathrm{d}}}e_{\mathrm{sd}}(k)-\frac{T_{\mathrm{c}}V_n{}^{\mathrm{d}}}{L_{\mathrm{d}}}] \\ &+\mathrm{j}[i_{\mathrm{sq}}^{\mathrm{ref}}-(1-\frac{T_{\mathrm{c}}R_{\mathrm{s}}}{L_{\mathrm{q}}})i_{\mathrm{sq}}(k)+\frac{T_{\mathrm{c}}}{L_{\mathrm{d}}}e_{\mathrm{sq}}(k)-\frac{T_{\mathrm{c}}V_n{}^{\mathrm{q}}}{L_{\mathrm{q}}}]\end{aligned} \tag{8b}$$

$$\boldsymbol{W}_{m'n}=\frac{V_{m'}{}^{\mathrm{d}}}{L_{\mathrm{d}}}-\frac{V_n{}^{\mathrm{d}}}{L_{\mathrm{d}}}+\mathrm{j}\frac{V_{m'}{}^{\mathrm{q}}}{L_{\mathrm{q}}}-\mathrm{j}\frac{V_n{}^{\mathrm{q}}}{L_{\mathrm{q}}} \tag{8c}$$

where $\boldsymbol{I}$ and $\boldsymbol{W}_{m'n}$ are two auxiliary vectors. The vector $\boldsymbol{I}$ is related to the sampling quantities, and the vector $\boldsymbol{W}_{m'n}$ uniquely corresponds to the voltage vector $\boldsymbol{v}_{m'n}$.

Substituting Eq.(8a) into Eq.(6) yields

$$g_n=\left|\boldsymbol{I}\right|^2-2t_{\mathrm{h}}\boldsymbol{I}\bullet\boldsymbol{W}_{m'n}+t_{\mathrm{h}}{}^2\left|\boldsymbol{W}_{m'n}\right|^2 \tag{9}$$

From Eq.(9), The objective function g_n with respect to the time duration t_{h} is a convey quadratic function. The condition of minimizing g_n with respect to t_{h} can be given by

$$\frac{\partial g_n}{\partial t_{\mathrm{h}}}=-2\boldsymbol{I}\bullet\boldsymbol{W}_{m'n}+2t_{\mathrm{h}}\left|\boldsymbol{W}_{m'n}\right|^2=0 \tag{10}$$

Solving Eq.(10) yields

$$t_{\mathrm{h}}{}^n=\frac{\boldsymbol{I}\bullet\boldsymbol{W}_{m'n}}{\left|\boldsymbol{W}_{m'n}\right|^2} \tag{12}$$

where the operator "•" means the dot product; $t_{\mathrm{h}}{}^n$ is the optimal time duration with respect to vector $\boldsymbol{v}_{m'n}$, as $t_{\mathrm{h}}{}^n\in[0,\ T_{\mathrm{c}}]$, if $t_{\mathrm{h}}{}^n$ is less than 0, then $t_{\mathrm{h}}{}^n$ should be limited as 0, if $t_{\mathrm{h}}{}^n$ is up to T_{c}, then $t_{\mathrm{h}}{}^n$ should be set as T_{c}.

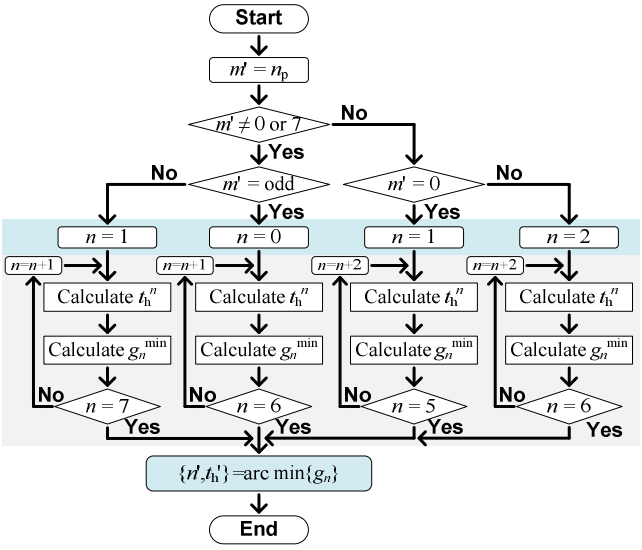

Fig. 3. Flowchart of the solving procedure.

Substituting every already t_h^n into Eq.(5), the objective functions g_n^{min} for all feasible n can be obtained. By evaluating all objective function values, the solution of Eq.(7) can be expressed as follows

$$\begin{cases} n' = \arg\min\{g_n^{\min}\} \\ t_h' = t_h^{n'} \end{cases} \tag{13}$$

where arg min$\{\bullet\}$ is the argument of the minimum.

The solving procedure can be represented as the flowchart shown in Fig.3. It can be seen that, by enumerating and evaluating all g_n^{min} over n=0,1,…,7, we can directly find the optimal solution [n', t_h']. It can be seen that the number of enumerations and evaluations is 8. Therefore, the above transformation of MPC optimization problem is more suitable for the discrete nature of digital processor.

C. Framework of the Proposed

The block diagram for the proposed approach is shown in Fig.4, which consists of the outer speed controller, DCS-MPC, coordinate-transformation and switching signal generator.

The outer speed controller is based on the linear PI control. Its transfer function is given by

$$G_{PI}(s) = K_p(1 + \frac{1}{\tau_i s}) \tag{14}$$

where K_p is proportional gain; τ_i is integration time constant.

The delay between the sampling instant and the instant of application of the new optimal actuation can be compensated by an oversampling method[10].

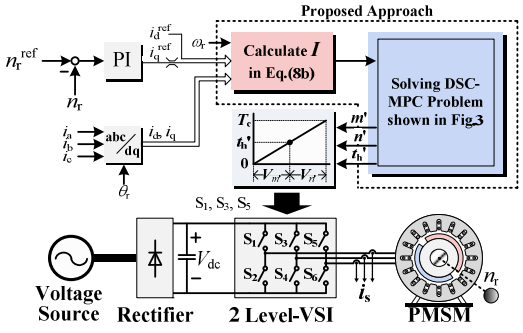

Fig. 4. FOC of the PMSM based on DCS-MPC.

TABLE I. RATED PARAMETERS OF PMSM

Parameter	Symbol	Value	Unit
Number of pole pairs	p	3	
Permanent magnet flux	ψ_f	0.2264	Wb
Stator resistance	R_s	0.25	Ω
d-axis inductance	L_d	3.3	mH
q-axis inductance	L_q	7.3	mH
Rated speed	n_N	1550	r/min
Rated torque	T_N	40	Nm
Rated voltage	U_N	230	V
Rated current	I_N	16.3	A
Rated frequency	f_N	77.5	Hz

To generate the switching signal, m' and n' will be translated into two switching states respectively. Moreover, an up-mode counter is required. The interaction of the saw wave and the switching instant t_h' will trigger a switching behavior between two selected switching states.

IV. SIMULATION ANALYSIS

In simulation, the parameters of PMSM are shown in Table I. The ripples of torque, d- and q-axis current can be evaluated by their standard deviation, which can be expressed as follows

$$\sigma_x = \sqrt{\frac{1}{m-1}\sum_{i=1}^{m}\left(x_i - \bar{x}\right)^2} \tag{15}$$

where $\bar{x} = \frac{1}{m}\sum_{i=1}^{m} x_i$; m is the number of samples.

The average switching frequency can be calculated as

$$f_{av} = \frac{\sum_{i=1}^{6} N_i}{6T} \tag{16}$$

where N_i is the total number of switching instances of the power switch S_i during a fixed period T, i=1, 2, ..., 6 and T=1s.

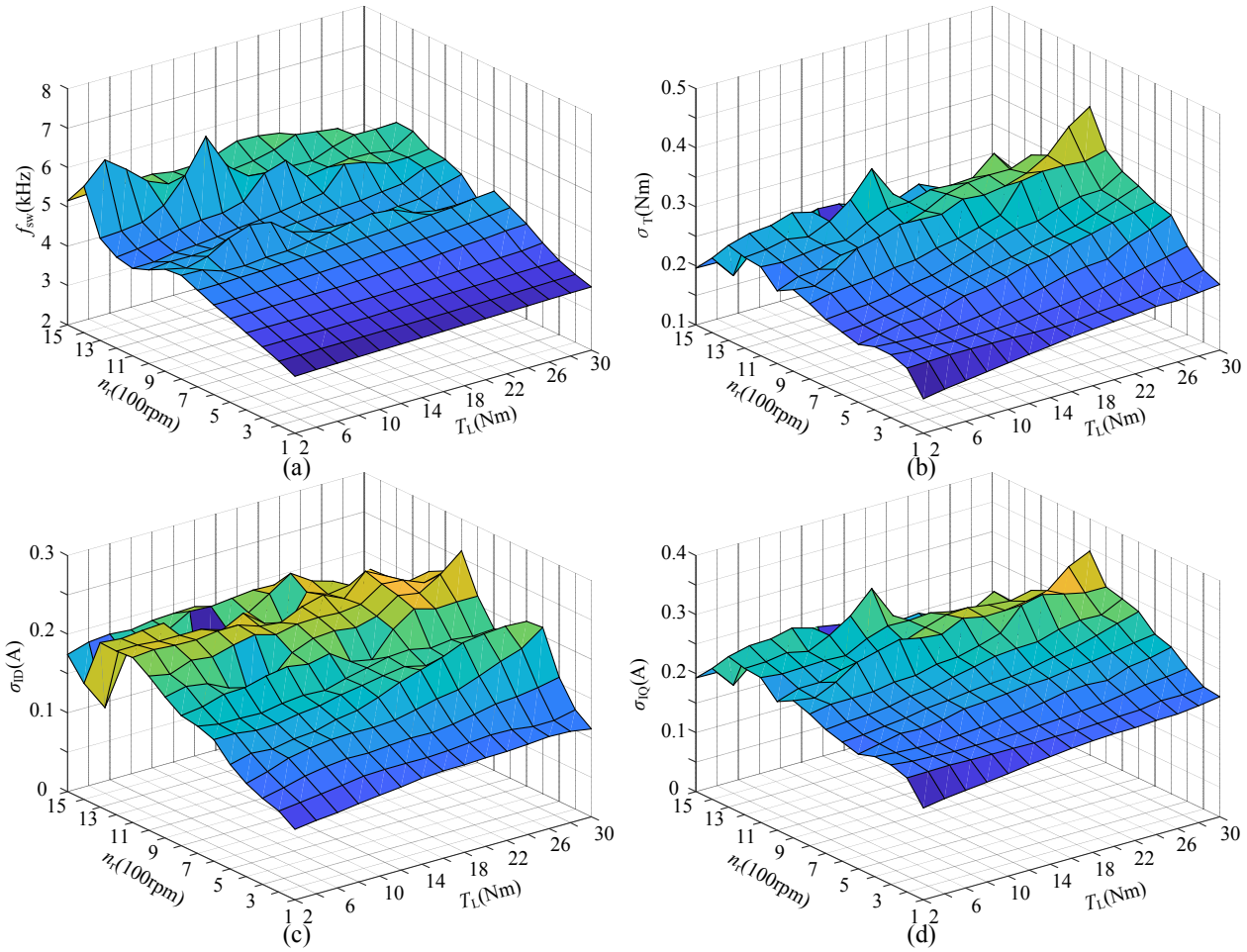

Fig. 5. Simulation results of the proposed approach with different speed n_r, load T_L. (a)switching frequency; (2) Standard deviation of torque; (b) Standard deviation of d-axis current; (c) Standard deviation of q-axis current.

Fig5 shows the switching frequency and standard deviation of torque, d- and q-axis current and flux in the proposed approach versus different speed n_r and load T_L. In simulation, the sampling frequency is equal to 20kHz, load torque T_L increases from 2Nm to 30Nm; speed n_r increases from 100r/min to 1000r/min.

From Fig.5(a), firstly, at low speed range, the switching frequency will be increased with speed, whereas the variation of T_L doesn't impact the switching frequency. But at high speed range, the switching frequency will approach smooth, but in some situation, the f_{sw} will be high. From Fig.5(b), (c), (d), at low speed and high speed range, the torque and current ripple are smaller than that at the middle speed range, while the variation of T_L doesn't impact the torque and current ripple except for some situations. Above test results shows that, under variable switching instant, the switching frequency will increase with the speed rather than load torque. The distribution of torque and current ripple are convey, at middle speed range, the torque and current ripples are higher. Moreover, from low to high speed, under variable switching instant, the maximum switching frequency is always lower than a third of sampling frequency.

V. Experimental Results

To verify the feasibility and effectiveness of the proposed approach, the experiments with a power rating 6.5kW PMSM are carried out in this section. The parameters of PMSM have been presented in Table I. The control system employs a TMS320F28335 DSP and an EP1C6 FPGA.

A. Tracking performance of the proposed approach

In this part, we investigate the tracking performance of the proposed approach alone, without the speed controller.

Fig.6 shows the waveforms of i_{sq}^{ref}, i_{sd} and i_{sq}^{ref}, i_{sd} for the proposed approach. In experiments, f_c=20kHz. In Fig.6(a), i_{sd}^{ref} is a step signal from 0A to −2A, and i_{sq}^{ref} is a step signal from 5A to 15A as well. It can be seen that the d-axis and q-axis currents can accurately track their references without overshoot or cross-coupling effects. It can be seen that the proposed approach has good track ability.

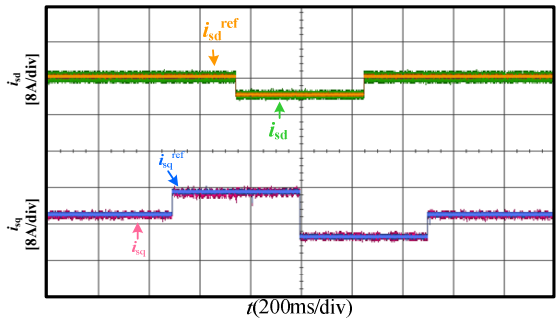

Fig. 6. Tracking performance of the proposed approach.

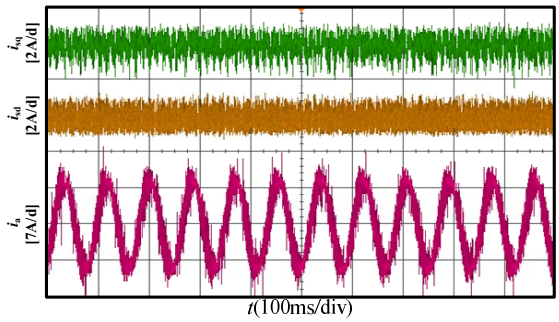

Fig. 7. Experimental waveforms of q-axis current, d-axis current, a-phase stator current, the harmonic spectrum of the current for FCS-MPC

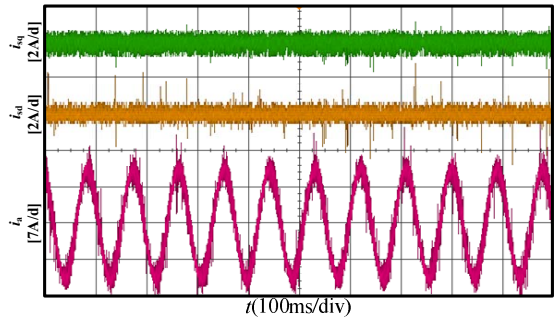

Fig. 8. Experimental waveforms of q-axis current, d-axis current, a-phase stator current, the harmonic spectrum of the current for MPC with Duty Cycle.

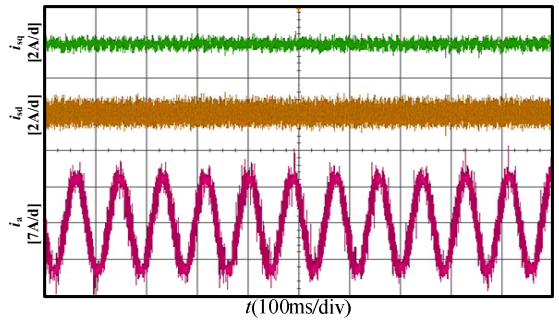

Fig. 9. Experimental waveforms of q-axis current, d-axis current, a-phase stator current, the harmonic spectrum of the current for the proposed approach

TABLE II. QUANTITATIVE COMPARISON OF THREE APPROACHES

Item	FCS-MPC	MPC with Duty Cycle	Proposed Approach
	Fig.7	**Fig.8**	**Fig.9**
f_{sam}(kHz)	20	20	20
f_{sw}(kHz)	3.218	8.176	**4.834**
σ_{ID}(A)	0.7129	0.5867	0.6721
σ_{IQ}(A)	0.5237	0.4317	0.1927

B. Comparison of FCS-MPC, MPC with duty cycle and the proposed approach

In experiments, three approaches are performed under the same operating point, where n_r=500r/min; T_L=10Nm.

From Fig.7, 8 and 9, under the same sampling frequency, the proposed approach can produce the stator current with lower harmonic distortion than two other approaches. From Table II, under the same sampling frequency, three approaches' switching frequencies are not the same. For FCS-MPC, only one switching state is employed within one sampling interval, so its switching frequency (f_{av}=3.218 kHz) is the lowest of three. In MPC with duty cycle, as 2 switching states appear within one sampling interval, its average switching frequency (f_{av}=8.176kHz) is higher than others. For the proposed approach, although variable switching instant allows 2 switching states within one sampling interval, switching behavior just appears at most one-time within one sampling interval, which leads to the proposed approach's switching frequency (f_{av}=4.834kHz) in the middle of the FCS-MPC's and MPC with duty cycle's switching frequency, and more approaching to the FCS-MPC.

VI. CONCLUSION

In this work, a novel Dynamic Control-Set Model Predictive Control has been proposed for VSI-PMSM drives. It provides an effect solution to mollify the contradiction between high steady-state performance and low switching frequency. Compared with the FCS-MPC, and its modified schemes, the proposed approach can achieve better steady-state performance, rather than result in higher switching frequency.

Moreover, in this work, variable switching instant has been illustrated from the view of space vector, which can help revealing the relationship between variable switching instant and PMSM's control variables. Based on it, the proposed approach can capture an optimal control action from infinite candidate control action via finite enumerations and evaluation online, which doesn't cost more computational effort. This kind of online optimization procedure distinguishes the proposed approach from already existing strategies. Furthermore, based on the proposed approach, more ideas for other kinds of drive systems are expected to be stimulated.

REFERENCES

[1] R. Krishnan, Permanent Magnet Synchronous and Brushless DC Motor Drives, Boca Raton: CRC Press, 2010.

[2] J. Rodriguez, Predictive Control of Power Converters and Electrical Drives, New York: Wiley, 2012.

[3] S. Wang, C. Xia, X. Gu, and W. Chen. "A novel FCS-model predictive control algorithm with duty cycle optimization for surface-mounted PMSM" 2014 *IET Power Electronics, Machines and Drives (PEMD 2014) Conf*. pp. 1-6.

[4] F. Morel, X. Lin-Shi, J.-M. Retif, B. Allard, and C. Buttay, "A comparative study of predictive current control schemes for a permanent-magnet synchronous machine drive," *IEEE Trans. Ind. Electron.*, vol. 56, no. 7, pp. 2715-2728, July. 2009.

[5] Y. Zhang, W. Xie, Z. Li, and Y. Zhang, "Model predictive direct power control of a PWM rectifier with duty cycle optimization," *IEEE Trans. Power Electron.,* vol. 28, no. 11, pp. 5343–5351, Nov. 2013.

[6] Z. Song, Y. Tian, W. Chen, Z. Zou and Z. Chen. "Predictive Duty Cycle Control of Three-Phase Active-Front-End Rectifiers" *IEEE Trans. Power Electron.*, vol. 31, no. 1 pp. 698-710. Jan 2016.

[7] M. Nemec, K. Drobnic, D. Nedeljkovic, and V. Ambrozic, "Direct current control of a synchronous machine in field coordinates," *IEEE Trans. Ind. Electron.*, vol. 56, no. 10, pp. 4052–4061, Oct. 2009.

[8] Y. Zhang and H. Yang, "Two-vector-based model predictive torque control without weighting factors for induction motor drives," *IEEE Trans. Power Electron*., vol. 31, no. 2, pp. 1381-1390, Feb. 2016.

[9] Y. Yan and S. Wang, etc. "Hybrid Control Set-Model Predictive Control for Field-Oriented Control of VSI-PMSM," *IEEE Trans. Energy Conversion*, vol. 31, no. 4, pp. 1622-1633, Aug. 2016.

[10] P. Cortes, J. Rodriguez, C. Silva and A. Flores, " Delay Compensation in Model Predictive Current Control of a Three-Phase Inverter," *IEEE Trans. Ind. Electron*., vol. 59, no. 2, pp. 1323–1325, May 2011.